Spacecraft Attitude Control Using Variable Inertia Reaction Wheels

Narottama Esser
University of Florida
Gainesville, FL
n.esser@ufl.edu

Faculty Advisor: Riccardo Bevilacqua
University of Florida

ABSTRACT

This paper examines the usefulness of variable inertia reaction wheels (VIRWs) for spacecraft attitude control as compared to traditional fixed inertia reaction wheels (FIRWs). The equations of motion were derived for a spacecraft with FIRWs and VIRWs. Quaternions were used to represent the spacecraft's orientation. A Lyapunov-based controller was derived and used to control the attitude quaternion and angular velocity of the spacecraft with the two control variables being the reaction wheels' inertia and angular acceleration. A Simulink/MATLAB simulation was created to test the response of the FIRWs and the VIRWs to spacecraft reorientation maneuvers and detumble maneuvers. The results showed that VIRWs performed better than the FIRWs when the VIRWs' inertia was allowed to increase beyond the inertia of the FIRWs. When the VIRWs' max inertia was limited to the inertia of the FIRWs then the FIRWs performed slightly better by reaching the desired attitude slightly faster. For a detumble maneuver the VIRWs required less total angular acceleration as the inertia of the wheels were decreased to slow down near the desired attitude rather than deaccelerating the wheels. Overall, the systems performed quite similarly when the VIRWs' max inertia was limited to the inertia of the FIRW.

INTRODUCTION

The purpose of this paper is to study the usage of variable inertia reaction wheels (VIRWs) in spacecraft attitude control.

There has not been much work done with VIRWs as the control systems and mechanical design of such a system are more complex compared to traditional fixed inertia reaction wheels (FIRWs). A paper by Christian *et al* described how a VIRW test platform was developed and tested in a microgravity environment and found that as the inertia of the reaction wheels was increased or decreased the precision of the attitude control decreased and increased, respectively. The precision was defined as the number of reaction wheel revolutions to rotate the spacecraft a degree.[1] Another paper by Wang *et al* focuses on developing a controller for spacecraft attitude control using VIRWs and through simulation finds that the resulting controller performs well and is capable of disturbance rejection.[2]

There has also been some research done on variable inertia flywheels (VIFs) and design ideas for them. The design ideas for VIFs could be used in creating a physical design for a VIRW. A paper by Ullman *et al* looks at some energy equations and possible designs for a VIF. The design ideas for varying the inertia of the wheel include: using a flexible coiled band that could be wrapped around the central shaft through a separate motor or allowed to move radially outwards through centrifugal forces, using magnetic particles suspended in a fluid matrix which can be attracted to the center with a magnet, as well as several other design concepts.[3] A patent filed by Lewis describes a VIF design where the inertia is varied by moving a lightweight piston radially through cylinders filled with a heavy, incompressible fluid.[4] A patent by Burstall describes another VIF design where the inertia is varied by pumping an electrolytic fluid radially through the use of an electromagnetic pump.[5]

To examine the usefulness of a VIRW system it is compared to a FIRW system. First, the equation of motion and control equation for a spacecraft with three orthogonal VIRWs are derived. Next, a simulation model of a spacecraft with VIRWs is created using MATLAB/Simulink. The same steps are repeated for a spacecraft with FIRWs. The results of the two simulations are then compared.

DIFFERENTIAL EQUATIONS OF MOTION

Fixed Inertia Reaction Wheels

First, the equations of motion were derived for a spacecraft with three orthogonal FIRWs with the spin axes of the reaction wheels aligned with the principal axes of the spacecraft. The inertia of reaction wheels around their spin axes was represented as a diagonal matrix, $\boldsymbol{I_s^W}$, where I_{s1}^W represented the inertia of the first reaction wheel around the spin axis aligned with the first principal axis of the spacecraft, and so on (Eq. 1).

$$\boldsymbol{I_s^W} = \begin{bmatrix} \boldsymbol{I_{s1}^W} & \mathbf{0} & \mathbf{0} \\ \mathbf{0} & \boldsymbol{I_{s2}^W} & \mathbf{0} \\ \mathbf{0} & \mathbf{0} & \boldsymbol{I_{s3}^W} \end{bmatrix} \quad \textbf{(1)}$$

To calculate the equation of motion for the spacecraft the conservation of angular momentum equation was used (Eq. 2).

$$\vec{H}_c = \boldsymbol{J_T}\vec{\omega}_B + \boldsymbol{I_s^W}\vec{\Omega} \quad \textbf{(2)}$$

In the above equation, $\vec{H}_C$ represents the angular momentum of the spacecraft around the center of mass, $\boldsymbol{J_T}$ represents the matrix of inertia of the entire spacecraft (including the reaction wheels) in its principal axes, $\vec{\omega}_B$ represents the angular velocity of the spacecraft expressed in a body-fixed coordinate system, and $\vec{\Omega}$ represents the angular velocity of the three reaction wheels around their spin axes.

Next, the derivative of the angular momentum was taken and set equal to external torques, $\vec{T}_B$, using Equation (3).[6]

$$\frac{{}^N d\vec{H}_c}{dt} = \frac{{}^B d\vec{H}_c}{dt} + \vec{\omega}_B \times \vec{H}_c = \vec{T}_B \quad \textbf{(3)}$$

Which resulted in Equation (4).

$$\vec{T}_B = \boldsymbol{J_T}\dot{\vec{\omega}}_B + \boldsymbol{I_s^W}\dot{\vec{\Omega}} + \boldsymbol{\omega_B^\times}\left(\boldsymbol{J_T}\vec{\omega}_B + \boldsymbol{I_s^W}\vec{\Omega}\right) \quad \textbf{(4)}$$

Where $\boldsymbol{\omega_B^\times}$ represents the three-by-three skew-symmetric matrix of $\vec{\omega}_B$ in Equation (4).

Rearranging Equation (4), the differential equation of motion for a spacecraft with FIRWs was obtained (Eq. 5).

$$\dot{\vec{\omega}}_B = \boldsymbol{J_T}^{-1}\left[\vec{T}_B - \boldsymbol{I_s^W}\dot{\vec{\Omega}} - \boldsymbol{\omega_B^\times}\left(\boldsymbol{J_T}\vec{\omega}_B + \boldsymbol{I_s^W}\vec{\Omega}\right)\right] \quad \textbf{(5)}$$

Variable Inertia Reaction Wheels

Next, the same process was repeated to obtain the equation of motion for a spacecraft with three VIRWs with the spin axes of the reaction wheels aligned with the principal axes of the spacecraft. Equations (1) and (2) still hold for VIRWs. Using Equation (3) the derivative of the angular momentum around the center of the mass was obtained (Eq. 6).

$$\vec{T}_B = \boldsymbol{J_T}\dot{\vec{\omega}}_B + \boldsymbol{\dot{J}_T}\vec{\omega}_B + \boldsymbol{I_s^W}\dot{\vec{\Omega}} + \boldsymbol{\dot{I}_s^W}\vec{\Omega} + \boldsymbol{\omega_B^\times}\left(\boldsymbol{J_T}\vec{\omega}_B + \boldsymbol{I_s^W}\vec{\Omega}\right) \quad \textbf{(6)}$$

Assuming that the reaction wheels' inertia is changing only in the radial direction around the spin axes, which are aligned with the spacecraft's principal axes, and there are no other inertia changes, then $\boldsymbol{\dot{J}_T}$ is equal to $\boldsymbol{\dot{I}_s^W}$. Making that simplification and rearranging the equation, the differential equation of motion for a spacecraft with VIRWs was obtained (Eq. 7).

$$\dot{\vec{\omega}}_B = \boldsymbol{J_T}^{-1}\left[\vec{T}_B - \boldsymbol{\dot{I}_s^W}(\vec{\omega}_B + \vec{\Omega}) - \boldsymbol{I_s^W}\dot{\vec{\Omega}} - \boldsymbol{\omega_B^\times}\left(\boldsymbol{J_T}\vec{\omega}_B + \boldsymbol{I_s^W}\vec{\Omega}\right)\right] \quad \textbf{(7)}$$

CONTROL EQUATIONS

For controller architecture Lyapunov-based control was selected so that global asymptotic stability of the attitude error could be achieved. Quaternions are used to represent the attitude of the spacecraft to avoid the singularities present with Euler angles. The attitude quaternion, $\boldsymbol{q}$, was defined as the following (Eq. 8).

$$\boldsymbol{q} = \begin{bmatrix} q_1 \\ q_2 \\ q_3 \\ q_4 \end{bmatrix} = \begin{bmatrix} \vec{q} \\ q_4 \end{bmatrix} \quad \textbf{(8)}$$

The relationship between $\vec{\omega}_B$ and $\dot{\boldsymbol{q}}$, the derivative of the attitude quaternion, is defined as the following equation (Eq. 9).[7]

$$\dot{\boldsymbol{q}} = 0.5\begin{bmatrix} 0 & \omega_{B3} & -\omega_{B2} & \omega_{B1} \\ -\omega_{B3} & 0 & \omega_{B1} & \omega_{B2} \\ \omega_{B2} & -\omega_{B1} & 0 & \omega_{B3} \\ -\omega_{B1} & -\omega_{B2} & -\omega_{B3} & 0 \end{bmatrix}\boldsymbol{q} \quad \textbf{(9)}$$

If a desired attitude quaternion, $\boldsymbol{q_d}$, is defined then the error quaternion, $\boldsymbol{q_e}$, can be calculated as follows (Eq. 10).

$$\boldsymbol{q_e} = \begin{bmatrix} \vec{e} \\ e_4 \end{bmatrix} = \begin{bmatrix} q_{d4} & q_{d3} & -q_{d2} & -q_{d1} \\ -q_{d3} & q_{d4} & q_{d1} & -q_{d2} \\ q_{d2} & -q_{d1} & q_{d4} & -q_{d3} \\ q_{d1} & q_{d2} & q_{d3} & q_{d4} \end{bmatrix}\boldsymbol{q} \quad \textbf{(10)}$$

A desired angular velocity, $\vec{\omega}_d$, and angular velocity error, $\vec{\omega}_e$, can also be defined as follows (Eq. 11).

$$\vec{\omega}_e = \vec{\omega}_B - \vec{\omega}_d \quad \textbf{(11)}$$

To track the desired angular velocity and desired attitude quaternion the following Lyapunov candidate function was chosen:

$$V = \frac{1}{2}\vec{\omega}_e^T \boldsymbol{J_T} \vec{\omega}_e + \vec{e}^T \vec{e} + (1 - e_4)^2 \quad (12)$$

Equation (12) is positive definite for all values of $\vec{\omega}_e$ and $\boldsymbol{q_e}$. To achieve asymptotic stability $\dot{V}$ must be negative definite. A desired $\dot{V}$ is defined in Equation (13).

$$\dot{V} = -\vec{\omega}_e^T \boldsymbol{K} \vec{\omega}_e \quad (13)$$

$\boldsymbol{K}$ is a positive gain matrix. Equation (13) is therefore negative definite for all $\vec{\omega}_e$. To ensure that $\boldsymbol{q_e}$ is also stable $\ddot{V}$ must be negative definite when $\vec{\omega}_e$ equals zero.

$$\ddot{V} = -2\vec{\omega}_e^T \boldsymbol{K} \dot{\vec{\omega}}_e \quad (14)$$

$$\ddot{V} = -2\dot{\vec{\omega}}_e^T \boldsymbol{K} \vec{\omega}_e - 2\vec{\omega}_e^T \boldsymbol{K} \dot{\vec{\omega}}_e \quad (15)$$

To check for stability for $\boldsymbol{q_e}$ a substitution was performed to include a function of $\boldsymbol{q_e}$. This substitution was performed by first taking the derivative of Equation (12) as follows:

$$\dot{V} = \tfrac{1}{2}\vec{\omega}_e^T \dot{\boldsymbol{J}}_{\boldsymbol{T}} \vec{\omega}_e + \vec{\omega}_e^T \boldsymbol{J_T} \dot{\vec{\omega}}_e + 2\vec{e}^T \dot{\vec{e}} - 2(1 - e_4)\dot{e}_4 \quad (16)$$

Using quaternion kinematic equations, the following equations were used to simplify $\dot{V}$ (Eq. 17, 18).[8]

$$\dot{\vec{e}} = \tfrac{1}{2}\boldsymbol{e}^{\times}\vec{\omega}_e + \tfrac{1}{2}e_4\vec{\omega}_e \quad (17)$$

$$\dot{e}_4 = -\tfrac{1}{2}\vec{e}^T\vec{\omega}_e \quad (18)$$

Substituting Equation (17) and (18) into Equation (16) and cancelling terms yields the following (Eq. 19).

$$\dot{V} = \vec{\omega}_e^T\left(\tfrac{1}{2}\dot{\boldsymbol{J}}_{\boldsymbol{T}}\vec{\omega}_e + \boldsymbol{J_T}\dot{\vec{\omega}}_e\right) + (\vec{e}^T\boldsymbol{e}^{\times} + \vec{e}^T)\vec{\omega}_e \quad (19)$$

Transposing the second half of the Equation (19) and simplifying yields the following equation (Eq. 20).

$$\dot{V} = \vec{\omega}_e^T\left(\tfrac{1}{2}\dot{\boldsymbol{J}}_{\boldsymbol{T}}\vec{\omega}_e + \boldsymbol{J_T}\dot{\vec{\omega}}_e + \vec{e}\right) \quad (20)$$

Setting Equation (20) equal to Equation (13) yields the following (Eq. 21).

$$-\vec{\omega}_e^T\boldsymbol{K}\vec{\omega}_e = \vec{\omega}_e^T\left(\tfrac{1}{2}\dot{\boldsymbol{J}}_{\boldsymbol{T}}\vec{\omega}_e + \boldsymbol{J_T}\dot{\vec{\omega}}_e + \vec{e}\right) \quad (21)$$

Next, $\vec{\omega}_e^T$ was cancelled on both sides of the equation and $\vec{\omega}_e$ was set equal to zero since the substitution into $\ddot{V}$ is looking for stability of $\boldsymbol{q_e}$ where $\vec{\omega}_e$ equals zero. Doing that resulted in the following equation (Eq. 22).

$$\dot{\vec{\omega}}_e = -\boldsymbol{J_T}^{-1}\vec{e} \quad (22)$$

Substituting Equation (22) into Equation (15) and setting $\vec{\omega}_e$ equal to zero gives the following equation for $\ddot{V}$ (Eq. 23).

$$\ddot{V} = -2\vec{e}^T\left(\boldsymbol{J_T}^{-1}\right)^{\boldsymbol{T}}\boldsymbol{K}\boldsymbol{J_T}^{-1}\vec{e} \quad (23)$$

Since all the matrixes in Equation (23) are positive definite, this proves $\ddot{V}$ is negative definite when $\vec{\omega}_e$ equals zero and therefore $\boldsymbol{q_e}$ is asymptotically stable.

With stability proven the control equation was then derived. Equation (21) was simplified and rearranged to produce the following equation (Eq. 24).

$$\vec{\omega}_B = -\boldsymbol{J_T}^{-1}\left(\tfrac{1}{2}\dot{\boldsymbol{J}}_{\boldsymbol{T}}\vec{\omega}_e + \vec{e} + \boldsymbol{K}\vec{\omega}_e - \boldsymbol{J_T}\dot{\vec{\omega}}_d\right) \quad (24)$$

To determine the control equation the differential equation of motion for VIRWs (Eq. 7) was substituted into Equation (24). The same simplification of $\dot{\boldsymbol{J}}_{\boldsymbol{T}}$ equal to $\dot{\boldsymbol{I}}_{\boldsymbol{s}}^{\boldsymbol{W}}$ as done in Equation (7) was made as well. Rearranging and simplifying results in the following control equation (Eq. 25).

$$\dot{\boldsymbol{I}}_{\boldsymbol{s}}^{\boldsymbol{W}}\boldsymbol{A} + \boldsymbol{I}_{\boldsymbol{s}}^{\boldsymbol{W}}\dot{\vec{\Omega}} = \boldsymbol{B} \quad (25)$$

Where:

$$\boldsymbol{A} = \tfrac{1}{2}\vec{\omega}_B + \tfrac{1}{2}\vec{\omega}_d + \Omega = \begin{bmatrix} A_1 \\ A_2 \\ A_3 \end{bmatrix} \quad (26)$$

$$\boldsymbol{B} = -\boldsymbol{J_T}\dot{\vec{\omega}}_d + \vec{e} + \boldsymbol{K}\vec{\omega}_e - \boldsymbol{\omega_B^{\times}}\left(\boldsymbol{J_T}\vec{\omega}_B + \boldsymbol{I}_{\boldsymbol{s}}^{\boldsymbol{W}}\vec{\Omega}\right) + \vec{T}_B \quad (27)$$

Since there are two unknown control variables in Equation (25), $\dot{\boldsymbol{I}}_{\boldsymbol{s}}^{\boldsymbol{W}}$ and $\dot{\vec{\Omega}}$, the method of Lagrange multipliers was used to solve for a constrained minimum solution. First, the controls solution, η, was defined as the following (Eq. 28).

$$\boldsymbol{\eta} = \begin{bmatrix} \dot{I}_{s1}^{W} \\ \dot{I}_{s2}^{W} \\ \dot{I}_{s3}^{W} \\ \dot{\Omega}_1 \\ \dot{\Omega}_2 \\ \dot{\Omega}_3 \end{bmatrix} \quad (28)$$

Which simplifies Equation (25) to the following (Eq. 29).

$$\boldsymbol{Q\eta = B} \tag{29}$$

Where $\boldsymbol{Q}$ is defined as the following:

$$\boldsymbol{Q} = \begin{bmatrix} A_1 & 0 & 0 & I_{s1}^W & 0 & 0 \\ 0 & A_2 & 0 & 0 & I_{s2}^W & 0 \\ 0 & 0 & A_3 & 0 & 0 & I_{s3}^W \end{bmatrix} \tag{30}$$

To produce a constrained minimum solution a diagonal gain matrix, $\boldsymbol{W}$, was created (Eq. 31) so that the solution variables can be weighted differently so that priority can be given to one control input over the other.

$$\boldsymbol{W} = \begin{bmatrix} W_1 & \cdots & 0 \\ \vdots & \ddots & \vdots \\ 0 & \cdots & W_6 \end{bmatrix} \tag{31}$$

To solve the constrained minimum solution the function that needs to be minimized, $f(\eta)$, was defined as the following (Eq. 32).

$$f(\boldsymbol{\eta}) = \tfrac{1}{2}\boldsymbol{\eta^T W^{-1} \eta} \tag{32}$$

The solution depends on Equation (29) being fulfilled, so the following constraint was set:

$$g(\boldsymbol{\eta}) = 0 = \boldsymbol{Q\eta - B} \tag{33}$$

The Lagrangian, $\mathcal{L}$, was therefore defined as the following (Eq. 34).

$$\mathcal{L} = \tfrac{1}{2}\boldsymbol{\eta^T W^{-1} \eta + \lambda^T (Q\eta - B)} \tag{34}$$

Where the Lagrange multiplier, $\boldsymbol{\lambda}$, which needs to be solved for was defined as the following (Eq. 35).

$$\boldsymbol{\lambda} = \begin{bmatrix} \lambda_1 \\ \lambda_2 \\ \lambda_3 \end{bmatrix} \tag{35}$$

Taking the derivative of $\mathcal{L}$ with respect to both $\boldsymbol{\lambda}$ and $\boldsymbol{\eta}$ and setting both derivatives equal to zero:

$$\frac{\partial \mathcal{L}}{\partial \boldsymbol{\eta}} = \boldsymbol{W^{-1}\eta + Q^T \lambda} = 0 \tag{36}$$

$$\frac{\partial \mathcal{L}}{\partial \boldsymbol{\lambda}} = \boldsymbol{Q\eta - B} = 0 \tag{37}$$

Solving the system of equations (Eq. 36, 37) for the Lagrange multiplier resulted in the following (Eq. 38).

$$\boldsymbol{\lambda = -(QWQ^T)^{-1} B} \tag{38}$$

Solving for the control variables, $\boldsymbol{\eta}$, results in the following equation (Eq. 39).

$$\boldsymbol{\eta = WQ^T (QWQ^T)^{-1} B} \tag{39}$$

Equation (39) represents the final control equation that was used to solve for the control variables $\boldsymbol{\dot{I}_s^W}$ and $\vec{\Omega}$ for a spacecraft with VIRWs.

To calculate the controls solution for a spacecraft with FIRWs Equation (25) was used but $\boldsymbol{\dot{I}_s^W}$ was set equal to zero since the reaction wheel inertia is fixed. That resulted in the following control solution for FIRWs (Eq. 40).

$$\boldsymbol{I_s^W \dot{\vec{\Omega}} = B} \tag{40}$$

SIMULATION

With the control solutions obtained for a spacecraft with both VIRWs and FIRWs, the equations of motion, control solutions, and quaternion kinematics were implemented into a Simulink/MATLAB model. The calculations for each equation were done through MATLAB function blocks and connected together. The angular acceleration of the spacecraft, the reaction wheel angular acceleration, the quaternion derivative, and the reaction wheel inertia change were all integrated through integrator blocks with external initial conditions set through MATLAB initialization code. The simulation for the FIRWs was created in a similar way without the reaction wheel inertia change. The FIRWs simulation was implemented as a subsystem in the main Simulink model so the two models could be compared.

All initial values were set through MATLAB initialization code. The maximum mass and dimensions of a NASA 6U CubeSat were used to calculate the inertia used to test the simulation. The maximum mass for a 6U CubeSat is 12kg and the maximum dimensions are $0.1\text{m} \times 0.226\text{m} \times 0.366\text{m}$.[9] Assuming an equal mass distribution of the CubeSat and approximating it as a rectangular box the inertia was calculated to be:

$$\boldsymbol{J_T} = \begin{bmatrix} 0.185 & 0 & 0 \\ 0 & 0.144 & 0 \\ 0 & 0 & 0.061 \end{bmatrix} kg \cdot m^2 \tag{41}$$

Reaction wheel specifications for the simulation were determined by looking at the specifications of a reaction wheel designed for 6U CubeSats from an online vendor.[10] The inertia of the reaction wheels

around their spin axes were set as the following for the simulation:

$$\boldsymbol{I_s^W} = 5.7 \times 10^{-5}[\mathbf{I}]_{3x3}\ kg \cdot m^2 \quad (42)$$

$[\mathbf{I}]_{3x3}$ represents a 3x3 identity matrix in Equation (42). The max angular velocity and acceleration were also calculated from the online vendor's specifications.[10] The max angular velocity for the reaction wheels was set at 2,106 rad/s or 20,111 rpm. The max angular acceleration was set at 176 rad/s. These two limits were implemented by using MATLAB code logic and capping the output of the control equations to those maximum numbers. Since there are no commercially available VIRWs nor any papers that describe the inertia varying capabilities of a reaction wheel, arbitrary constraints were placed on the max inertia, minimum inertia, and max rate of change of inertia of the VIRWs. The inertia range was set to $\boldsymbol{I_{s_{min}}^W} = (1 \times 10^{-5})[\mathbf{I}]_{3x3}\ kg \cdot m^2$ and $\boldsymbol{I_{s_{max}}^W} = (1 \times 10^{-4})[\mathbf{I}]_{3x3}\ kg \cdot m^2$. The max rate of change of inertia was set to $(5 \times 10^{-5})\ \frac{kg \cdot m^2}{s}$. The inertia limitations were implemented in the same way as the angular velocity and acceleration constraints. The constant gain matrix $\boldsymbol{K}$ was set equal to $\mathbf{2} \times [\mathbf{I}]_{3x3}$ for all the performed simulations except the second scenario (Figure 3) where the $\boldsymbol{K}$ gain was tuned to better compare the two reaction wheel systems. The constant gain matrix, $\boldsymbol{W}$, represents the relation between the two control variables. To balance the output of the control equations the $\boldsymbol{W}$ gain matrix was set to the following:

$$\boldsymbol{W} = \begin{bmatrix} 1[\mathbf{I}]_{3x3} & \mathbf{0}_{3x3} \\ \mathbf{0}_{3x3} & 1 \times 10^{14}[\mathbf{I}]_{3x3} \end{bmatrix} \quad (43)$$

$\mathbf{0}_{3x3}$ represents a 3x3 matrix of zeroes in Equation (43).

Although the desired angular velocity and desired angular acceleration could be set to varying values to produce a better response from the controller, for the following simulations they were set equal to zero. All other initial conditions were also set equal to zero unless mentioned otherwise.

The Simulink model used to perform the simulation can be seen below (Figure 1).

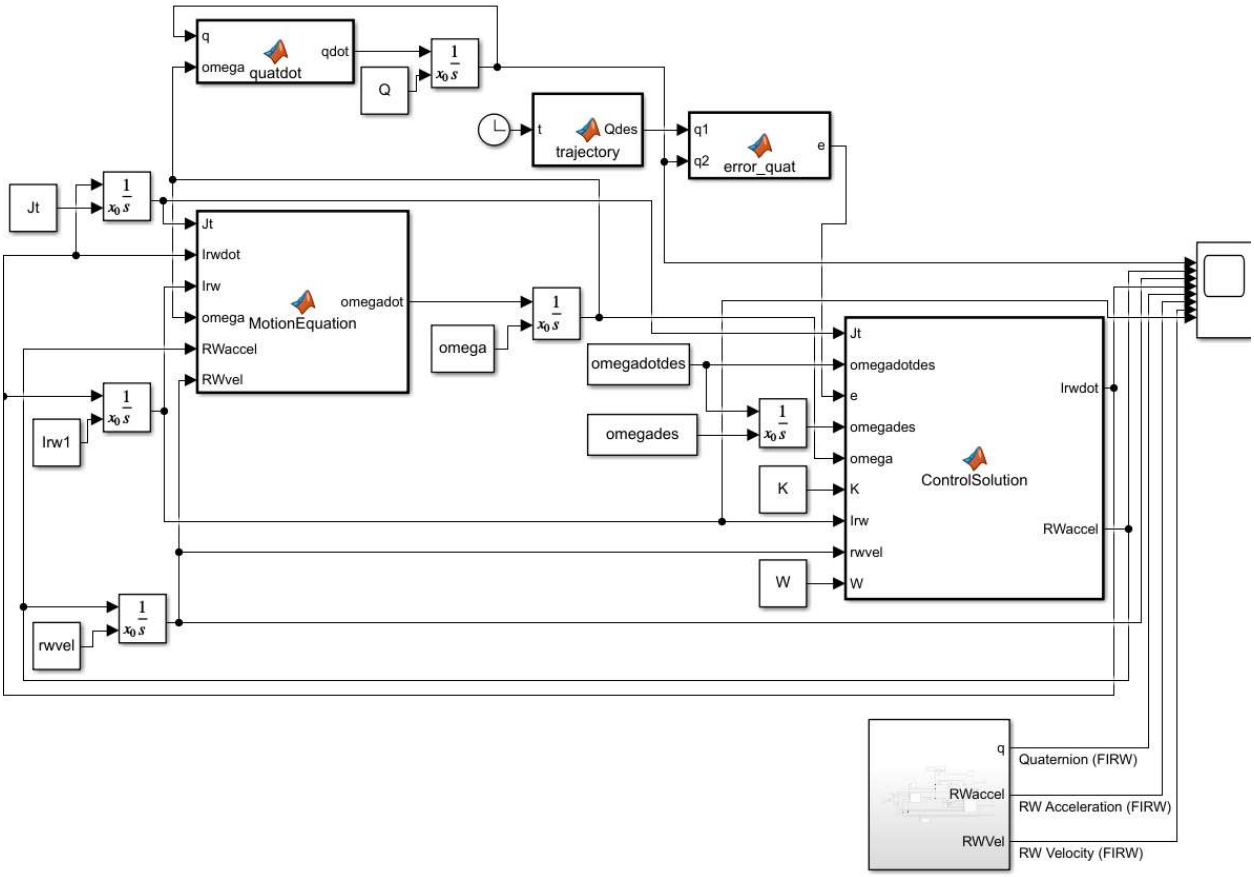

Figure 1: Simulink Model

RESULTS

Attitude Adjustment Maneuver

The first scenario tested through the Simulink model was a simple attitude adjustment: changing the attitude quaternion, $\boldsymbol{q}$, from the initial condition of [0;0;0;1] to the desired quaternion of [1;0;0;0]. This quaternion change represents a spacecraft rotation of 180 degrees. The same initial conditions stated in the previous section remained the same. The resulting graphs for both the FIRWs and VIRWs can be seen below (Figure 2).

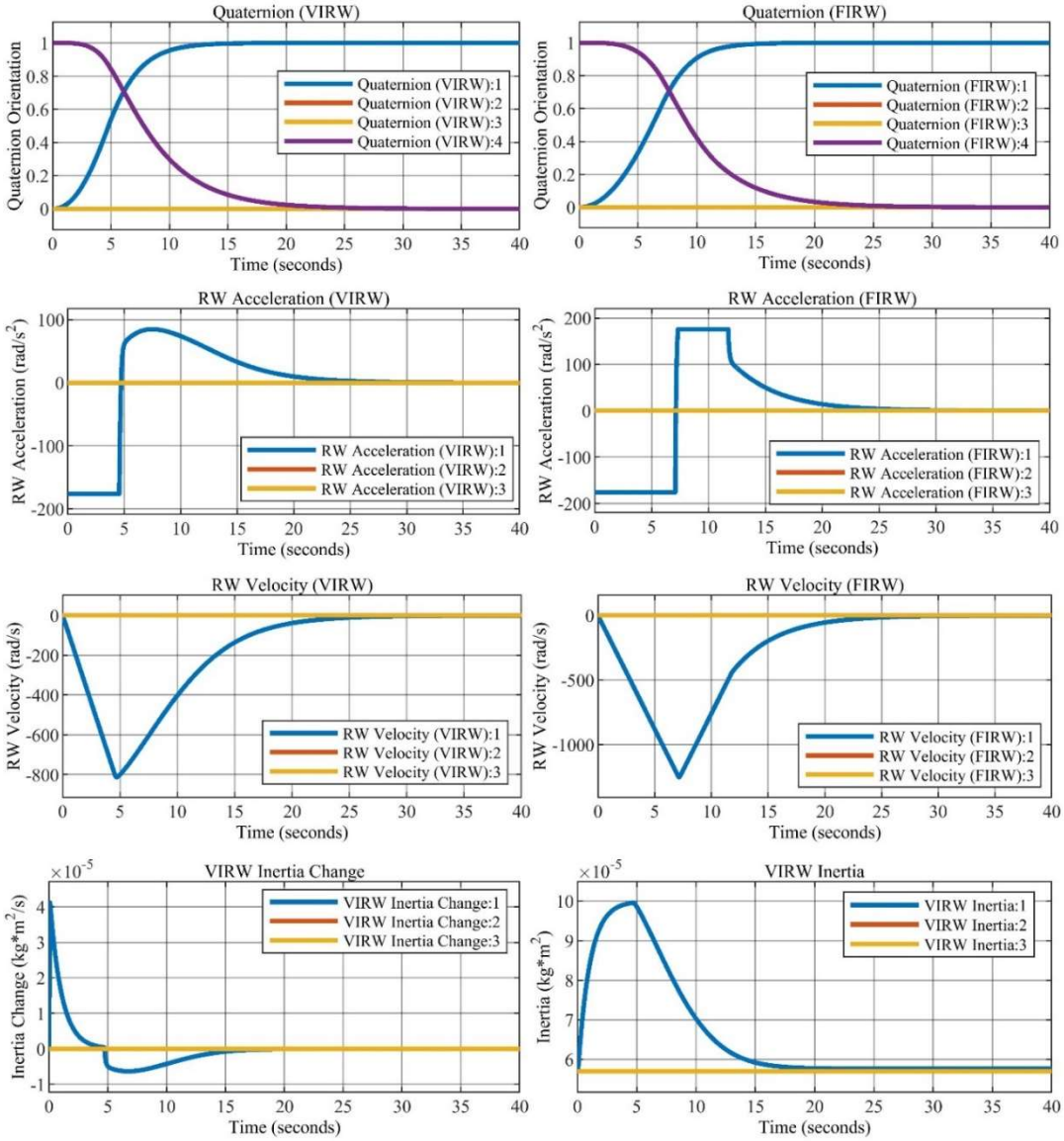

Figure 2: Attitude Adjustment Maneuver Simulation Results

The top six graphs of Figure 2 compare the quaternion attitude values, the reaction wheels' (RW) angular accelerations, and the RWs' angular velocities for both the FIRWs and the VIRWs. The two graphs below show the rate of change of the inertia and the inertia values for the VIRWs. It can be seen from the results that the VIRWs produce a quicker attitude adjustment response, require less RW acceleration, and require less RW velocity to perform the maneuver. Looking at the bottom right graph the VIRWs reach the max inertia values and it is due to this increased inertia that the response is better.

Attitude Adjustment Maneuver with Same Max Reaction Wheel Inertia

The same maneuver as the previous section was performed but with several changes made. Since the VIRWs reached higher inertia values it was able to

perform better at carrying out the previous maneuver. In this scenario the FIRWs' inertia was increased to the max inertia value allowed for the VIRWs: $\boldsymbol{I}_{s_{max}}^{W} = (1 \times 10^{-4})[\mathbf{I}]_{3x3}\ kg \cdot m^2$. This inertia increase was also added to the total spacecraft inertia for the FIRWs to account for the larger reaction wheels. The $\boldsymbol{K}$ gain matrix was tuned for both systems to obtain the best responses with no overshoot. This was done to compare both systems' optimal responses for a reorientation maneuver. The $\boldsymbol{K}$ gain matrix was set to $\mathbf{1.10} \times [\mathbf{I}]_{3x3}$ for the VIRWs and $\mathbf{1.31} \times [\mathbf{I}]_{3x3}$ for the FIRWs. The remaining initial conditions remained the same. The simulation produced the following results for these conditions (Figure 3).

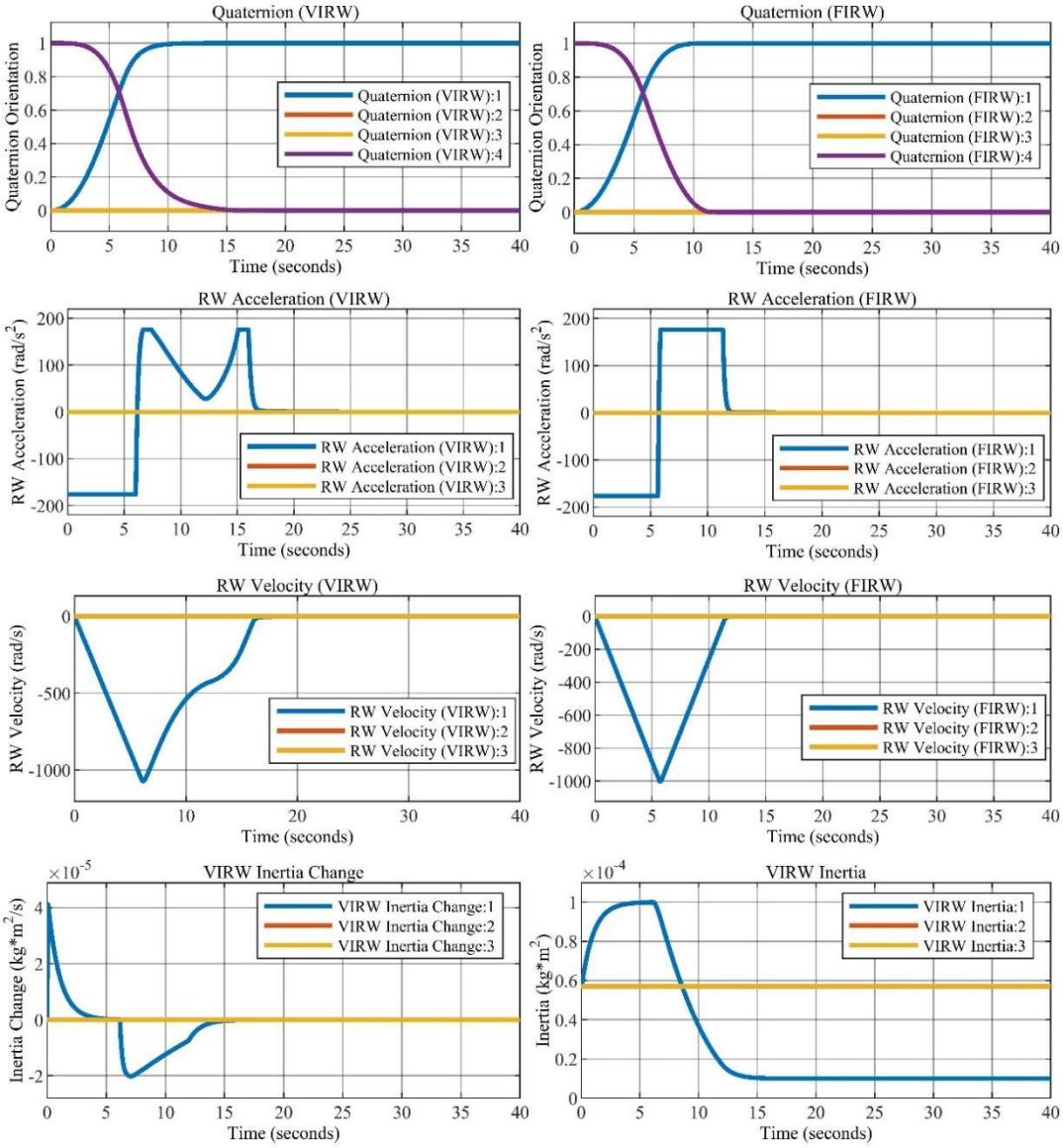

Figure 3: Attitude Adjustment Maneuver with Same Max Reaction Wheel Inertia

It can be seen from Figure 3 that when the inertia of the FIRWs were set to the max value of inertia for the VIRWs it resulted in the FIRWs taking slightly less time to reach the desired orientation. The VIRWs performed similar to the FIRWs by first increasing the inertia of the reaction wheels to the max to perform the maneuver quickly and when it neared the desired attitude it reduced the inertia of the wheels to reduce the spacecraft angular velocity. The FIRWs performed slightly better with this specific reorientation maneuver as well as other tested reorientation maneuvers.

Detumble Maneuver

Normally detumble maneuvers are not performed using reaction wheels but a detumble maneuver was

simulated just to see if VIRWs could perform better than FIRWs and perhaps make detumbling using reaction wheels a valid option. Since it was determined from Figure 2 that the VIRWs reached higher inertia values and performed better mostly just because of that, for this maneuver the FIRWs were again set to have the same inertia as the max inertia allowed for the VIRWs: $\boldsymbol{I_{s_{max}}^{W}} = (1 \times 10^{-4})[\mathbf{I}]_{3x3}\ kg \cdot m^2$. This additional inertia was also added to the total inertia of the FIRW spacecraft to account for the larger reaction wheels. The constant gain matrix $\boldsymbol{K}$ was set to $\mathbf{2} \times [\mathbf{I}]_{3x3}$. The $\boldsymbol{W}$ gain matrix was modified for this scenario to give more priority to the variable inertia control variable as can be seen below (Eq. 44).

$$\boldsymbol{W} = \begin{bmatrix} 1[\mathbf{I}]_{3x3} & \mathbf{0}_{3x3} \\ \mathbf{0}_{3x3} & 1 \times 10^{12}[\mathbf{I}]_{3x3} \end{bmatrix} \quad (44)$$

For this scenario, the angular velocity of the spacecraft was set to 5 rpm on all axes and the desired quaternion was set equal to the same as the initial quaternion: [0;0;0;1]. The simulation result can be seen below (Figure 4).

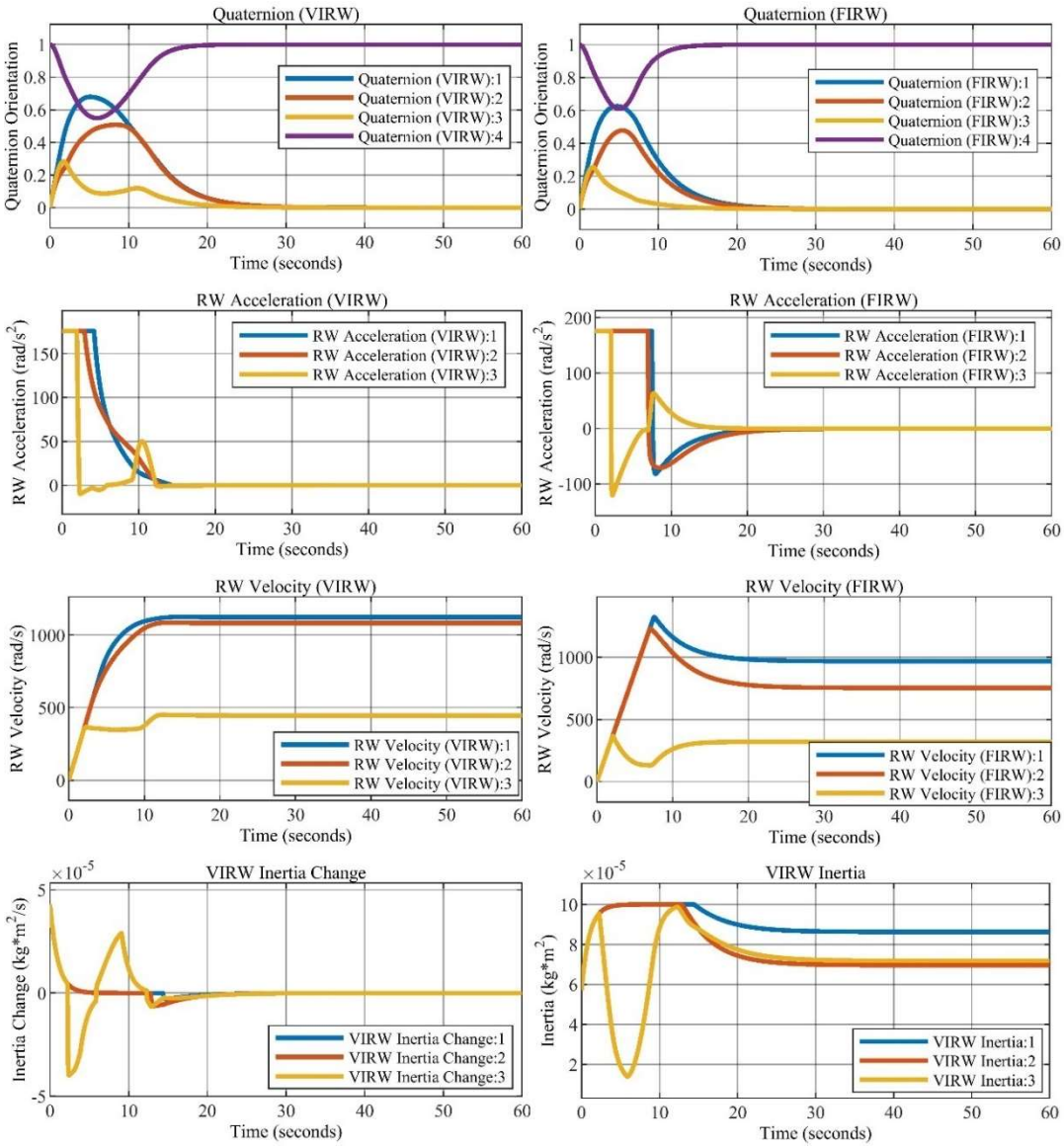

Figure 4: Detumble Maneuver Results

Figure 4 shows that the FIRWs produced a quicker response to the desired quaternion and were able to cancel out the spacecraft angular velocity faster than the VIRWs. The VIRWs required less overall acceleration to perform the maneuver. This was because as the spacecraft reached the desired attitude

the inertia of the wheels decreased to slow the spacecraft's angular velocity rather than deaccelerating the reaction wheels. While the FIRWs peaked at a higher velocity, they ended up stabilizing the spacecraft at a lower final velocity compared to the VIRWs as the inertia decreased for the VIRWs at the end instead of decreasing the velocity. If a detumble maneuver was performed with reaction wheels the final reaction wheel velocity could slowly be eliminated using a magnetorquer. However, the VIRWs performed similarly to the FIRWs for a detumble maneuver so the VIRWs do not provide a distinct advantage that would make reaction wheels a more viable option for detumble maneuvers.

CONCLUSION

The results from the simulation show various advantages and disadvantages of using VIRWs compared to FIRWs for spacecraft attitude control. The results of Figure 2 show that VIRWs with a greater inertia capability compared to the inertia of the FIRWs will perform better at a simple reorientation maneuver due to the higher inertia capability. The results of Figure 3 show that if FIRWs have the same inertia as the max inertia possible for the VIRWs then the VIRWs will perform slightly worse than the FIRWs by taking slightly longer to reach the desired attitude. The results of Figure 4 show that for a detumble maneuver where the FIRWs have the same inertia as the max inertia possible for the VIRWs then the VIRWs take longer to cancel out the angular velocity but also require less total angular acceleration and a lower peak angular velocity.

In most other scenarios where the FIRWs have the same inertia as the max possible inertia for the VIRWs, the FIRWs will perform the same or slightly better than the VIRWs. However, one advantage which was not tested through the simulation was the precision of the attitude control. As found by Christian *et al* the VIRWs are able to produce more precise attitude control when the inertia of the reaction wheels is decreased.[1] VIRWs with the derived control system in this paper could perform better than FIRWs in certain scenarios as well as having additional precision in attitude control.

If further work were to be done on this topic, then improvements to the simulation could be made such as implementing some way to simulate the real-world precision of attitude control. There could also be further improvements on the control system such as dynamically adjusting the desired angular velocity and acceleration of the reaction wheels to produce a better response. A VIRW test platform could also be made similar to the work done by Christian *et al* that instead uses the control system derived in this paper that dynamically adjusts the inertia of reaction wheels to improve the response rather than changing the inertia of the reaction wheels manually.[1]

REFERENCES

1. Christian, J., Turbe, M., Kabo, E., Manno, L., and Johnson, E., "Development of a Variable Inertia Reaction Wheel System for Spacecraft Attitude Control," AIAA 2004-5132. AIAA Guidance, Navigation, and Control Conference and Exhibit. August 2004. https://doi.org/10.2514/6.2004-5132.
2. Wang, Z., Dong, W., Yang, Z., and Tong, C., "Characteristic model and attitude control based on Golden-section control law for small satellite," 2015 7th International Conference on Modelling, Identification and Control (ICMIC), Sousse, Tunisia, 2015, pp. 1-6, doi: 10.1109/ICMIC.2015.7409435.
3. Ullman, D., and Velkoff, H., "An Introduction to the Variable Inertia Flywheel (VIF)." ASME. J. Appl. Mech. March 1979; 46(1): 186–190. https://doi.org/10.1115/1.3424494.
4. Lewis, O. G., U.S. Patent No. 3,248,967, 1966, U.S. Patent Office.
5. Burstall, Oliver W. J., U.S. Patent No. 6,883,399, 2005, U.S. Patent Office.
6. Rao, A. V., "Dynamics of Particles and Rigid Bodies: A Systematic Approach", Cambridge: Cambridge University Press, 2006, pp. 410-411.
7. Tewari, A., "Atmospheric and Space Flight Dynamics: Modeling and Simulation with MATLAB and Simulink", Boston, MA: Birkhäuser Boston, 2007, pp. 37–38.
8. Markley, F. L., and Crassidis, J. L., "Fundamentals of Spacecraft Attitude Determination and Control", Springer, 2016, pp. 355–359.
9. The CubeSat Program, Cal Poly SLO, "6U CubeSat Design Specification Revision 1.0," https://www.cubesat.org/, June 2018. [Online]. Available:https://static1.squarespace.com/static/5418c831e4b0fa4ecac1bacd/t/5b75dfcd70a6adbee5908fd9/1534451664215/6U_CDS_2018-06-07_rev_1.0.pdf. [Accessed: March 2021].
10. Sinclair Interplanetary, "Microsatellite Reaction Wheels (RW3-0.06)," https://www.rocketlabusa.com/, 2015. [Online]. Available:https://www.rocketlabusa.com/assets/Uploads/60-MNMS-product-sheet.pdf. [Accessed: March 2021].